Modeling Study of the Effects of Overlapping Ca^{2+} Microdomains on Neurotransmitter Release

Richard Bertram,* Gregory D. Smith,# and Arthur Sherman#
*School of Science and Center for Mathematical Biology, Pennsylvania State University, Erie, Pennsylvania 16563, and
#Mathematical Research Branch, National Institute of Diabetes and Digestive and Kidney Diseases, National Institutes of Health, Bethesda, Maryland 20892 USA

ABSTRACT Although single-channel Ca^{2+} microdomains are capable of gating neurotransmitter release in some instances, it is likely that in many cases the microdomains from several open channels overlap to activate vesicle fusion. We describe a mathematical model in which transmitter release is gated by single or overlapping Ca^{2+} microdomains produced by the opening of nearby Ca^{2+} channels. This model accounts for the presence of a mobile Ca^{2+} buffer, provided either that the buffer is unsaturable or that it is saturated near an open channel with Ca^{2+} binding kinetics that are rapid relative to Ca^{2+} diffusion. We show that the release time course is unaffected by the location of the channels (at least for distances up to 50 nm), but paired-pulse facilitation is greater when the channels are farther from the release sites. We then develop formulas relating the fractional release following selective or random channel blockage to the cooperative relationship between release and the presynaptic Ca^{2+} current. These formulas are used with the transmitter release model to study the dependence of this form of cooperativity, which we call Ca^{2+} current cooperativity, on mobile buffers and on the local geometry of Ca^{2+} channels. We find that Ca^{2+} current cooperativity increases with the number of channels per release site, but is considerably less than the number of channels, the theoretical upper bound. In the presence of a saturating mobile buffer the Ca^{2+} current cooperativity is greater, and it increases more rapidly with the number of channels. Finally, Ca^{2+} current cooperativity is an increasing function of channel distance, particularly in the presence of saturating mobile buffer.

INTRODUCTION

Neurotransmitter release from synaptic terminals is accomplished through the fusion of transmitter-filled vesicles with the presynaptic plasma membrane. The importance of Ca^{2+} in this process was first demonstrated by Katz and Miledi (1968), and has since been elaborated. Briefly, upon membrane depolarization Ca^{2+} enters the presynaptic terminal through voltage-gated channels. Although the majority of this Ca^{2+} is quickly bound by endogenous buffers (Neher and Augustine, 1992), some will reach and bind to Ca^{2+} acceptors at transmitter release sites located at or near the plasma membrane. The identity of these acceptors is not clear, but the vesicle-bound protein synaptotagmin has been implicated (Brose et al., 1992; Davletov and Südhof, 1993; Geppert et al., 1994; Südhof and Rizzo, 1996). Studies demonstrating a fourth-power relation between transmitter release and the external Ca^{2+} concentration suggest that vesicle fusion requires the binding of at least four Ca^{2+} ions to one or more fusion proteins (Augustine and Charlton, 1986; Borst and Sakmann, 1996; Dodge and Rahamimoff, 1967; Stanley, 1986). Ca^{2+} imaging of high-concentration Ca^{2+} microdomains located near transmitter release sites (Llinás et al., 1992), and the rapidity of transmitter release following the opening of Ca^{2+} channels (Llinás et al., 1981b; Sabatini and Regehr, 1996) argue in favor of the colocalization of Ca^{2+} channels and release sites. Further evidence for colocalization has been provided by the finding that release can be evoked by the opening of a single Ca^{2+} channel (Augustine et al., 1991; Stanley, 1993; Yoshikami et al., 1989). Taken together, these findings suggest that release is gated primarily by the microdomains of high Ca^{2+} concentration that form at nearby open Ca^{2+} channels. Although more remote channels can contribute, we consider their effect only indirectly through their contribution to bulk Ca^{2+}.

There have been numerous mathematical studies of the Ca^{2+} distribution near an open Ca^{2+} channel or within a presynaptic terminal (Aharon et al., 1994, 1996; Cooper et al., 1996; Fogelson and Zucker, 1985; Issa and Hudspeth, 1996; Klingauf and Neher, 1997; Naraghi and Neher, 1997; Neher, 1986; Simon and Llinás, 1985; Sinha et al., 1997; Smith et al., 1996; Stern, 1992; Winslow et al., 1994). These studies show that the Ca^{2+} microdomain at the mouth of a channel forms quickly upon opening of the channel and dissipates quickly upon channel closure, reaching equilibrium within microseconds (Simon and Llinás, 1985). In two studies, formulas were developed for the equilibrium Ca^{2+} profile near an open channel (Neher, 1986; Smith, 1996). These formulas relate the Ca^{2+} concentration to the distance from the channel, and differ primarily in the treatment of Ca^{2+} buffers. One formula (the "excess buffer approximation") is based on the assumption that the buffer is unsaturable (Neher, 1986), while the other (the "rapid buffer approximation") is valid for buffers that are saturated near an open channel and have Ca^{2+} binding kinetics that are

Received for publication 1 December 1997 and in final form 9 September 1998.

Address reprint requests to Dr. Richard Bertram, School of Science, Pennsylvania State University, Erie, PA 16563. Tel.: 814-898-6090; Fax: 814-898-6213; E-mail: bertram@euler.bd.psu.edu.

0006-3495/99/02/735/16 $2.00

rapid relative to Ca^{2+} diffusion (Naraghi and Neher, 1997; Smith, 1996).

In the present report we couple these formulas for the steady-state domain Ca^{2+} concentration to a model of transmitter release based on the cooperative binding of Ca^{2+} to four acceptors or gates at the release sites. This model was originally formulated with the assumption that each release site is located at a fixed small, but indeterminate, distance from a single Ca^{2+} channel, and that the release site is influenced by no more than one channel (Bertram et al., 1996; Bertram, 1997). By coupling this to either formula for the steady-state domain Ca^{2+} we extend the model in three ways: the Ca^{2+} channel can now be placed at different distances from the release site, the bulk Ca^{2+} concentration is introduced into the model, and the effects of endogenous and exogenous buffers on transmitter release can now be studied. The first extension is important because the free Ca^{2+} concentration drops off quickly with distance from the channel and the influence of Ca^{2+} buffers depends greatly on the diffusional distance. The second extension is important because during long impulse trains the bulk Ca^{2+} can accumulate, and may be a factor in augmentation, a form of synaptic enhancement longer than the facilitation considered herein (Delaney et al., 1989; Swandulla et al., 1991). Inasmuch as we do not look at long trains in this report, we make the assumption that the bulk Ca^{2+} concentration is constant in time. The third extension is important because endogenous Ca^{2+} buffers are ubiquitous in synaptic terminals, and exogenous buffers are often used to image the Ca^{2+} concentration or to alter transmitter release.

If two or more channels are open simultaneously in the vicinity of a release site, then the Ca^{2+} microdomains can overlap, increasing the probability of vesicle fusion. The extent of overlap in synaptic terminals depends on many factors, including the local geometry of channels; the types of Ca^{2+} channels; the duration and degree of depolarization; and the concentration and kinetics of any endogenous and exogenous buffers. Evidence for the involvement of Ca^{2+} domain overlap in action-potential-evoked release has been provided in several preparations, including hippocampal CA3 to CA1 synapses (Wheeler et al., 1994), granule cell to Purkinje cell synapses (Mintz et al., 1995), and calyces of Held (Borst and Sakmann, 1996). Conversely, there have been reports that domain overlap is not necessary for or does not contribute significantly to action potential-evoked release in the squid giant synapse (Augustine, 1990), the frog neuromuscular junction (Yoshikami et al., 1989), or calices of the chick ciliary ganglion (Stanley, 1993). In any case, the many factors that can influence Ca^{2+} domain overlap allow for the dynamic control of the extent of overlap within a given synapse, and thus for the dynamic modulation of release from the synapse.

The excess buffer and rapid buffer approximations for steady-state domain Ca^{2+} concentration were formulated for Ca^{2+} influx through a single channel. We extend these steady-state formulas to describe the Ca^{2+} concentration in the vicinity of multiple open channels. This allows us to further extend the transmitter release model to the case of overlapping Ca^{2+} microdomains from multiple nearby Ca^{2+} channels. Although there are restrictions (described below), the extended release model can be used with multiple channels per release site placed at different distances from the site, and in the absence or presence of Ca^{2+} buffers. Because a formula for the local steady-state Ca^{2+} concentration is used rather than a time-dependent reaction-diffusion equation, the release model is simple to use and to analyze. In addition, it is formulated to take into account Ca^{2+} channel kinetics, a feature found in some modeling studies of transmitter release (Bennett et al., 1995, 1997; Bertram et al., 1996; Simon and Llinás, 1985), but not others.

Assumptions underlying the steady-state domain Ca^{2+} formulas place restrictions on the transmitter release model. Both formulas are valid only near a Ca^{2+} source, where the Ca^{2+} concentration is expected to quickly reach equilibrium. This is perhaps most restrictive in the case of release evoked by Ca^{2+} from multiple channels, all of which must lie within $\sim$50 nm of the release site for the steady-state domain Ca^{2+} formulas to apply. Although it has not been possible to determine the channel geometry in most synapses, there are examples of such a close association of channels in large synapses (Cooper et al., 1996; Haydon et al., 1994; Heuser et al., 1974). Simulations of the effects of buffers are restricted either to high buffer concentrations or to buffers that bind Ca^{2+} rapidly, such as BAPTA, fura-2, or calmodulin (Pethig et al., 1989; Falke et al., 1994). Thus, analysis of the effects of larger structures such as overlapping Ca^{2+} macrodomains from adjacent active zones (Cooper et al., 1996) or of slow buffers such as EGTA is beyond the scope of the present model.

One ubiquitous feature of synaptic transmission is the enhancement of release in response to a train of two or more closely spaced presynaptic impulses. One type of short-term enhancement, facilitation, is produced in the present release model by the slow unbinding of Ca^{2+} from three of the four release gates. This was discussed in detail for a precursor release model (Bertram et al., 1996; Bertram, 1997; Bertram and Sherman, 1998). In the present report we examine the effects on facilitation and the shape of the release time course of channel location. We find that increasing the channel distance (which decreases Ca^{2+} concentration at the release site) increases facilitation, but does not alter the shape of the release time course. This is analogous to findings that decreasing the external Ca^{2+} concentration increases facilitation (Rahamimoff, 1968; Charlton and Bittner, 1978; Stanley, 1986), while leaving the release time course unchanged (Borst and Sakmann, 1996; Datyner and Gage, 1980).

We next investigate the effects on transmitter release of both selective and random Ca^{2+} channel blockage. This is motivated by experimental studies in which channel blockers such as ω-conotoxins, ω-agatoxins, ω-grammotoxin, and various divalent cations were used to selectively or randomly block Ca^{2+} channels in presynaptic terminals, reduc-

ing or eliminating transmitter release (Luebke et al., 1993; Mintz et al., 1995; Regehr and Mintz, 1994; Smith and Cunnane, 1997; Turner et al., 1993; Wheeler et al., 1994; Wu and Saggau, 1995). In several of these studies a determination was made of whether or not Ca^{2+} microdomain overlap contributes significantly to release. This was done either by checking if the individual inhibitory effects of different toxins (acting selectively on different Ca^{2+} channel types) sum to a value exceeding 100%, or by determining the exponent of the power law relating transmitter release to the Ca^{2+} current (i.e., the Ca^{2+} *current cooperativity*). A Ca^{2+} current cooperativity of one indicates single-domain release, while a cooperativity greater than one indicates multidomain release. This form of cooperativity reflects the distribution of Ca^{2+} channels contributing to transmitter release. Another form of cooperativity, Ca_{ex} cooperativity, is measured by varying the external Ca^{2+} concentration, and reflects the number of Ca^{2+} binding sites in the release mechanism. Throughout this report, "cooperativity" refers to Ca^{2+} current cooperativity, unless stated otherwise.

We derive formulas relating Ca^{2+} current cooperativity to the fractional reduction of release following channel blockage, and through these formulas show that the channel number is the upper bound on this form of cooperativity. We then use the release model to investigate the dependence of Ca^{2+} current cooperativity on factors such as channel distance, the number of channels per release site, and the presence of a mobile buffer. We find that the Ca^{2+} current cooperativity increases with the number of channels per site, although this increase is less than expected from the theoretical upper bound. Surprisingly, the Ca^{2+} current cooperativity is relatively insensitive to channel distance, at least for distances of 50 nm or less. The presence of a fast-binding saturating mobile buffer increases the Ca^{2+} current cooperativity for any arrangement of channels and release sites. It also increases the rate of rise of Ca^{2+} current cooperativity with the number of Ca^{2+} channels per site, and introduces a positive dependence of cooperativity on the channel distance. These effects are caused by buffer saturability, since they are not observed in the presence of an unsaturable buffer.

Although the cooperative relation between the presynaptic Ca^{2+} current and transmitter release provides useful information about the structural properties of synapses, it can lead to some paradoxical results, which we discuss later. This is to be expected because the Ca^{2+} current is a macroscopic measure of the Ca^{2+} influx throughout the terminal regardless of channel location, and transmitter release is an event gated by local Ca^{2+} channel openings. Hence, some care must be taken in the interpretation of experimental measurements of the Ca^{2+} current cooperativity of release.

In this report we begin with a description of a simple version of the transmitter release model, with one Ca^{2+} channel per release site. To extend this model to the case of more than one channel per site, we next derive formulas for the Ca^{2+} concentration near clustered open channels. This is followed by extensions of the release model to two channels per site, and to M equidistant channels per site. Using these multichannel release models, the effects of the local channel geometry on facilitation and the release time course are then discussed. Next, formulas for the Ca^{2+} current cooperativity are developed. Finally, these formulas are used in conjunction with the multichannel release models to test the sensitivity of release and Ca^{2+} current cooperativity to the local channel geometry and the presence of buffers.

SINGLE-CHANNEL RELEASE MODEL

An experimental determination of the kinetic scheme for Ca^{2+} binding at release sites has not been made. Previous models of transmitter release have assumed that Ca^{2+} acceptors are independent and identical (Fogelson and Zucker, 1985); independent with different Ca^{2+} affinities and kinetic rates (Bertram et al., 1996; Yamada and Zucker, 1992); or that binding is sequential with non-cooperative kinetics (Bennett et al., 1995, 1997) or with cooperative kinetics (Heidelberger et al., 1994). Note that in this context "cooperative" refers to the kinetics of Ca^{2+} binding to release sites. In our earlier studies we used an independent binding scheme, but switch now to a sequential scheme that substantially reduces the number of equations required to describe release when more than one channel is associated with each release site. The simplest form of the scheme is

$$S_0 \underset{k_1^-}{\overset{4k_1^+\mathrm{Ca}}{\rightleftharpoons}} S_1 \underset{2k_2^-}{\overset{3k_2^+\mathrm{Ca}}{\rightleftharpoons}} S_2 \underset{3k_3^-}{\overset{2k_3^+\mathrm{Ca}}{\rightleftharpoons}} S_3 \underset{4k_4^-}{\overset{k_4^+\mathrm{Ca}}{\rightleftharpoons}} S_4$$

where S_j represents a release site with j Ca^{2+} ions bound and Ca is the Ca^{2+} concentration at the release site. A more realistic scheme would have the release site return to the completely unbound state, S_0, following fusion. However, simulations incorporating the $S_4 \rightarrow S_0$ transition produce quantitatively similar results during the short impulse trains considered in this study (not shown). We have neglected this refinement for simplicity.

In our kinetic scheme, we choose graded Ca^{2+} unbinding rates $k_4^- \gg k_3^- > k_2^- > k_1^-$. With these rates, unbinding of the first Ca^{2+} ion from the release site is rapid, ending the release process immediately upon termination of the presynaptic stimulus. Unbinding of additional ions is progressively slower. A slow unbinding mechanism of this type may be the basis of short-term facilitation (Bertram et al., 1996; Stanley, 1986; Yamada and Zucker, 1992), and the different unbinding time constants may be responsible for the several components of facilitated release observed experimentally (see Magleby, 1987 for review).

This simple sequential scheme is suitable when Ca is a given function of time, but we would like to capture the dependence of microdomain Ca^{2+} on the channel kinetics. Previously this was achieved using a Monte Carlo simulation for the stochastic channel kinetics (Bertram et al., 1996). However, if one enlarges the binding scheme so that each state represents both the state of the channel and the number of ions bound, a set of deterministic differential equations is obtained whose solution is the mean of the Monte Carlo process (Bertram and Sherman, 1998).

We begin with the simplest case of one channel per release site (Fig. 1), assuming that the Ca^{2+} channel has a single open state and a single closed state. The enlarged binding scheme is

$$\begin{array}{ccccccccc}
S_0^0 & \underset{k_1^-}{\overset{4\kappa_1^0}{\rightleftharpoons}} & S_1^0 & \underset{2k_2^-}{\overset{3\kappa_2^0}{\rightleftharpoons}} & S_2^0 & \underset{3k_3^-}{\overset{2\kappa_3^0}{\rightleftharpoons}} & S_3^0 & \underset{4k_4^-}{\overset{\kappa_4^0}{\rightleftharpoons}} & S_4^0 \\
\beta_x \updownarrow \alpha_x & & \beta_x \updownarrow \alpha_x & & \beta_x \updownarrow \alpha_x & & \beta_x \updownarrow \alpha_x & & \beta_x \updownarrow \alpha_x \\
S_0^1 & \underset{k_1^-}{\overset{4\kappa_1^1}{\rightleftharpoons}} & S_1^1 & \underset{2k_2^-}{\overset{3\kappa_2^1}{\rightleftharpoons}} & S_2^1 & \underset{3k_3^-}{\overset{2\kappa_3^1}{\rightleftharpoons}} & S_3^1 & \underset{4k_4^-}{\overset{\kappa_4^1}{\rightleftharpoons}} & S_4^1
\end{array}$$

where S_j^p represents a release site with j ions bound and with the associated Ca^{2+} channel closed ($p = 0$) or open ($p = 1$). For notational simplicity we

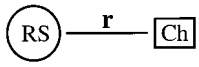

FIGURE 1 In the single-channel release model each release site (RS) is associated with a single Ca^{2+} channel (Ch), located at a distance r from the site.

also use S_j^p to denote the probability that the release site/channel complex is in this state. When $p = 0$, the release site senses the bulk cytoplasmic Ca^{2+}, and when $p = 1$ it senses the Ca^{2+} in the single-channel domain (which is influenced by the bulk cytoplasmic Ca^{2+}, see next section). The top row represents Ca^{2+} binding/unbinding when the channel is closed, while the bottom row is associated with an open channel. The channel opening and closing rates are α_x and β_x, respectively (see Appendix). The forward binding rate κ_j^p is the product of k_j^+ and the Ca^{2+} concentration at the release site (*Ca*) with the channel closed ($p = 0$) or open ($p = 1$). Either of the single channel domain Ca^{2+} formulas discussed later (Eqs. 23 or 31) may be used to compute *Ca*. The binding rates used are (in $ms^{-1}\ \mu M^{-1}$): $k_1^+ = 9.375 \times 10^{-4}$, $k_2^+ = 1.25 \times 10^{-3}$, $k_3^+ = 1.875 \times 10^{-3}$, and $k_4^+ = 3.75 \times 10^{-3}$. The unbinding rates are (in ms^{-1}): $k_1^- = 4 \times 10^{-4}$, $k_2^- = 5 \times 10^{-4}$, $k_3^- = 3.33 \times 10^{-2}$, $k_4^- = 2.5$. These rates were chosen to capture certain features of data from the squid giant synapse (Bertram et al., 1996; Stanley, 1986). They are used here as an illustrative case in which slow unbinding kinetics give rise to facilitation. Contrasts with other sets of kinetic rates are considered later.

Using the law of mass action, the binding scheme for transmitter release is described by the following differential equations:

$$\frac{dS_0^p}{dt} = k_1^- S_1^p - 4\kappa_1^p S_0^p + F_0^p \tag{1}$$

$$\frac{dS_1^p}{dt} = 4\kappa_1^p S_0^p + 2k_2^- S_2^p - (k_1^- + 3\kappa_2^p) S_1^p + F_1^p \tag{2}$$

$$\frac{dS_2^p}{dt} = 3\kappa_2^p S_1^p + 3k_3^- S_3^p - (2k_2^- + 2\kappa_3^p) S_2^p + F_2^p \tag{3}$$

$$\frac{dS_3^p}{dt} = 2\kappa_3^p S_2^p + 4k_4^- S_4^p - (3k_3^- + \kappa_4^p) S_3^p + F_3^p \tag{4}$$

$$\frac{dS_4^p}{dt} = \kappa_4^p S_3^p - 4k_4^- S_4^p + F_4^p, \tag{5}$$

for $p = 0$ and 1. The term $F_j^p = (-1)^p(\beta_x S_j^1 - \alpha_x S_j^0)$ describes the transition from a closed channel state to an open channel state, or vice versa. Since release occurs only when all four gates are bound, the probability of release is $R = S_4^0 + S_4^1$. Initial conditions for these equations are determined by allowing the system to equilibrate at the resting membrane potential (−65 mV).

The number of differential equations used to describe release can be reduced from 10 to 8 by noting that the sum of the states in the top row of the kinetic diagram is equal to the probability that the channel is closed, while the sum of the states in the bottom row is equal to the probability that the channel is open. That is,

$$S_0^0 + S_1^0 + S_2^0 + S_3^0 + S_4^0 = 1 - x \tag{6}$$

$$S_0^1 + S_1^1 + S_2^1 + S_3^1 + S_4^1 = x, \tag{7}$$

where x is the open probability of the channel, described by Eq. 66.

The numerical solution to this system is shown in Fig. 2. For simplicity we use S_j to denote the sum $S_j^0 + S_j^1$. In this figure release is evoked by four closely spaced action potentials, generated by the Hodgkin-Huxley equations (see Appendix). Each action potential produces a spikelike increase in *Ca*, resulting in rapid transitions from S_0–S_3 to the release state S_4. When

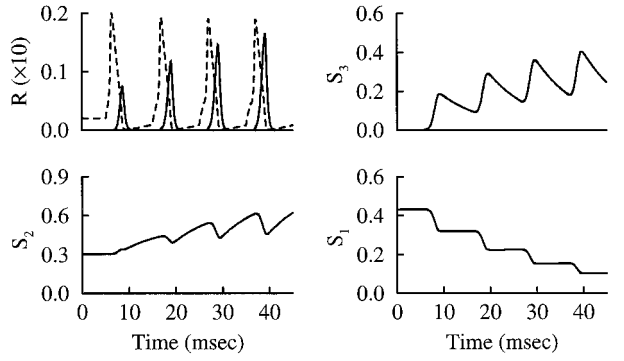

FIGURE 2 Numerical solution of Eqs. 1–5, 61–64, and 66. Here $R = S_4^0 + S_4^1$ and $S_j = S_j^0 + S_j^1$. Four closely spaced action potentials (*dashed curves, scaled*) elicit facilitated release due to the slow growth of S_2 and S_3. Each release site is associated with a single Ca^{2+} channel located 10 nm away. No mobile buffers are present. All numerical solutions were obtained using a Gear method with tolerance 10^{-9}.

Ca returns to its baseline value there is a rapid transition from S_4 to the nonreleasing state S_3 (since k_4^- is large), quickly terminating release. However, the backward transitions $S_3 \rightarrow S_2$, $S_2 \rightarrow S_1$, and $S_1 \rightarrow S_0$ are progressively slower, allowing S_2 and S_3 to accumulate during the short impulse train. This leads to facilitated release, where release is greater with each successive impulse. The bulk Ca^{2+} concentration is fixed at 0.1 μM in this and all subsequent simulations, so the facilitation is caused entirely by residual bound Ca^{2+}. However, for longer impulse trains a differential equation should be included for the bulk Ca^{2+} concentration, because with this protocol one would expect significant bulk Ca^{2+} accumulation. This higher bulk Ca^{2+} would generate residual binding between impulses, contributing to the enhancement of release (Bertram et al., 1996).

The number of differential equations describing release can be further reduced from eight to four by assuming that all the release sites see the average of the domain Ca^{2+} at all the channels. This captures some aspects of the channel kinetics and can be a useful simplifying approximation (Bertram, 1997; Bertram and Sherman, 1998), but it is unsuitable here because it averages out the effects of multiple channels. That is, it does not distinguish between variations in Ca^{2+} concentration resulting from an altered flux per channel versus an altered number of open channels. We extend the present model to the case of multiple channels per release site below, after first deriving formulas for the domain Ca^{2+} concentration near clusters of open channels.

STEADY-STATE Ca^{2+} CONCENTRATION FORMULAS

Both the single-channel release model and the multichannel model described later make use of the colocalization of release sites and Ca^{2+} channels that appears to prevail in most synapses. Hence, a formula is needed for determining the Ca^{2+} concentration near one or more open channels, which should be at steady state (Simon and Llinás, 1985). In a recent mathematical study of Ca^{2+} diffusion near an open Ca^{2+} channel (Smith, 1996), a formula was developed for the steady-state spatial profile of free Ca^{2+} in the presence of mobile buffers with rapid binding kinetics. The "rapid buffer approximation" (RBA) used to derive this formula is valid when Ca^{2+} buffer kinetics are fast relative to the diffusional time scale and when the buffer is saturated near an open channel. When the RBA is valid, this steady-state formula gives an upper bound on the Ca^{2+} profile, and near an open channel it provides an estimate of the domain Ca^{2+} concentration soon after channel activation.

We first re-derive the RBA near a single open channel given by Smith (1996). The new derivation uses a change of variables that makes the steady-state equation linear and thus allows its extension to the case of multiple sources (i.e., Ca^{2+} channels) by superposition.

We start by following the derivation of the time-dependent RBA as in Wagner and Keizer (1994). The reaction scheme for each mobile buffer species is

$$B_m + Ca^{2+} \underset{k_m^-}{\overset{k_m^+}{\rightleftharpoons}} CaB_m$$

Stationary buffers do not contribute to the steady-state profile of free Ca^{2+}, so we do not include them explicitly. Stationary buffers would contribute to the time-dependence of the Ca^{2+} concentration, particularly the bulk Ca^{2+}. However, for the short time spans considered in this report the bulk Ca^{2+} concentration is nearly constant, so we hold it fixed at its resting value.

Letting $Ca = [Ca^{2+}]$, $B_m^* = [CaB_m]$, and B_m^T be the total concentration of the buffer species, so that $B_m^T - B_m^*$ is the concentration of unbound buffer, the transport equations for Ca^{2+} and B_m^* are

$$\frac{\partial Ca}{\partial t} = D_c \nabla^2 Ca - k^+(B_m^T - B_m^*)Ca + k^- B_m^* \tag{8}$$

$$\frac{\partial B_m^*}{\partial t} = D_m \nabla^2 B_m^* + k^+(B_m^T - B_m^*)Ca - k^- B_m^*, \tag{9}$$

with an equation like Eq. 9 for each buffer species. Here D_c and D_m are the diffusion coefficients for free Ca^{2+} and for Ca^{2+} bound to buffer, respectively.

Next, let $Ca_T = Ca + B_m^*$, the total of free and bound Ca^{2+}. The transport equation for Ca_T is obtained by summing Eqs. 8 and 9:

$$\frac{\partial Ca_T}{\partial t} = D_c \nabla^2 Ca + D_m \nabla^2 B_m^*; \tag{10}$$

this is equivalent to Eq. 7 in Wagner and Keizer (1994).

We now define a new variable w, which is the sum of free and bound Ca^{2+}, weighted by their diffusion coefficients:

$$w = D_c Ca + D_m B_m^* \tag{11}$$

so that

$$\frac{\partial Ca_T}{\partial t} = \nabla^2 w. \tag{12}$$

Using the chain rule, this can be rewritten as a nonlinear diffusion equation for w, with a diffusion coefficient that depends on Ca:

$$\frac{\partial w}{\partial t} = [D_c \beta + D_m(1 - \beta)]\nabla^2 w, \tag{13}$$

where

$$\beta = \left(1 + \frac{K_m B_m^T}{(K_m + Ca)^2}\right)^{-1}. \tag{14}$$

Equations 13 and 14 are equivalent to the time-dependent RBA derived by Wagner and Keizer (1994). Sneyd et al. (1998) derived a transformation equivalent to Eq. 11 and obtained Eqs. 13 and 14 by directly seeking to remove the nonlinear transport term from the Wagner-Keizer formulation.

Here we focus on the steady-state solution to Eq. 13, which satisfies

$$\nabla^2 w = 0, \tag{15}$$

plus boundary conditions representing the sources (Ca^{2+} channels) at the plasma membrane and Ca in the interior of the cell. Note that we have reduced the steady-state RBA to the *linear* Poisson equation, so that we can handle multiple sources by superposition, but first we recover the formula of Smith for a single source. In this case, we can immediately write down the solution of the Poisson equation with hemispherical symmetry:

$$w = \frac{C_1}{r} + C_2, \tag{16}$$

where r is the distance from the source and where C_1, C_2 will be determined by the boundary conditions.

In order to recover Ca from w we now use for the first time the assumption of rapid buffering by imposing *local equilibrium*: that is, at every point in space, Ca^{2+} and buffer are assumed to be equilibrated and therefore related by

$$B_m^* = \frac{CaB_m^T}{K_m + Ca}, \tag{17}$$

where $K_m = k_m^-/k_m^+$ is the mobile buffer dissociation constant. Note that the steady states of the RBA are *not* in general steady states of the full system, Eqs. 8 and 9, because near sources steady-state solutions of the full equations do not necessarily satisfy the condition of local equilibrium. However, the steady-state RBA is equivalent to the steady state of the full system when conditions for the validity of the time-dependent RBA are met (Smith et al., 1996).

Finally, combining Eq. 17 with the boundary conditions

$$\lim_{r\to\infty} Ca = Ca_{bk} \tag{18}$$

and

$$\lim_{r\to 0} -2\pi r^2 \nabla w = \sigma, \tag{19}$$

where Ca_{bk} is the background or bulk Ca^{2+} concentration in the terminal and σ is the source strength (see Appendix), gives

$$D_c Ca + D_m \frac{CaB_m^T}{K_m + Ca} = \frac{\sigma}{2\pi r} + D_c Ca_{bk} + D_m \frac{Ca_{bk} B_m^T}{K_m + Ca_{bk}}. \tag{20}$$

This generalizes immediately in the case of multiple mobile buffers to

$$D_c Ca + \sum_i D_i \frac{CaB_i^T}{K_i + Ca} = \frac{\sigma}{2\pi r} + D_c Ca_{bk} + \sum_i D_i \frac{Ca_{bk} B_i^T}{K_i + Ca_{bk}}. \tag{21}$$

Equation 21 can be shown to be equivalent to Eq. 10 in Smith (1996) through the identity

$$B_i^T = \frac{K_i B_i^T}{K_i + Ca} + \frac{CaB_i^T}{K_i + Ca}. \tag{22}$$

As shown in Appendix B of Smith (1996), when there is only one mobile buffer Eq. 21 reduces to a quadratic equation for Ca whose solution is

$$Ca = \left(-D_c K_m + \frac{\sigma}{2\pi r} + \Psi + \sqrt{\left(D_c K_m + \frac{\sigma}{2\pi r} + \Psi\right)^2 + 4 D_c D_m B_m^T K_m}\right)/(2D_c), \tag{23}$$

where $\Psi = D_c Ca_{bk} - D_m B_m^T K_m/(K_m + Ca_{bk})$. The parameter values related to mobile buffers and to Ca^{2+} diffusion used in this report are given in Table 1.

In the case of multiple sources Eq. 16 generalizes to

$$w = \sum_j^M \frac{C_j}{r_j} + C_{M+1}, \tag{24}$$

where r_j is the distance from the jth Ca^{2+} source. Letting $\xi = \sqrt{r_1^2 + r_2^2 + \cdots + r_M^2}$, the boundary conditions (Eq. 18 and 19) also generalize:

$$\lim_{\xi \to \infty} Ca = Ca_{bk} \tag{25}$$

and

$$\lim_{r_j \to 0} -2\pi r_j^2 \nabla w = \sigma_j, \quad (j = 1, \ldots, M). \tag{26}$$

With multiple sources and multiple mobile buffers Eq. 21 generalizes to

$$D_c Ca + \sum_i D_i \frac{Ca B_i^T}{K_i + Ca} = \sum_j \frac{\sigma_j}{2\pi r_j} + D_c Ca_{bk} + \sum_i D_i \frac{Ca_{bk} B_i^T}{K_i + Ca_{bk}}. \tag{27}$$

With only one mobile buffer, Eq. 27 reduces to

$$Ca = (-D_c K_m + \Theta + \Psi + \sqrt{(D_c K_m + \Theta + \Psi)^2 + 4 D_c D_m B_m^T K_m})/(2D_c), \tag{28}$$

where

$$\Theta = \frac{1}{2\pi} \sum_{j=1}^M \frac{\sigma_j}{r_j}. \tag{29}$$

If the channel at r_j is closed, then $\sigma_j = 0$. If the channel is open, then σ_j is proportional to the influx of Ca^{2+} through the channel (see Appendix). In this report we assume that the channels are identical, so the σ_j for open channels are equal.

The multiple-source RBA (Eq. 27), like the single-source RBA, is a good approximation when the buffers are not only rapid but saturate near open channels. It shares with the single-source RBA the limitation that it can only be used in conditions where the steady state is achieved rapidly in comparison to other processes, i.e., in a small neighborhood of a tight cluster of Ca^{2+} channels. A complementary approximation due to Neher can be used when buffer is present in excess and cannot be saturated. In this case, a steady-state formula is obtained by setting $\partial Ca/\partial t = 0$ in the "excess buffer approximation" (EBA):

$$\partial Ca/\partial t = D_c \nabla^2 Ca - k_m^+ B_m^T (Ca - Ca_{bk}) + \sigma \delta(r), \tag{30}$$

where $\delta(r)$ is the Dirac delta function (Neher, 1986; Smith, 1996). Solving the steady-state equation for Ca,

$$Ca = \frac{\sigma}{2\pi D_c r} \exp(-r/\lambda) + Ca_{bk} \tag{31}$$

where $\lambda = \sqrt{D_c/(k_m^+ B_m^\infty)}$ and $B_m^\infty = K_m B_m^T/(K_m + Ca_{bk})$. The term λ is a characteristic length for binding of Ca^{2+} to the mobile buffer (Neher, 1986). This expression for λ corrects an error in Smith (1996).

Since Eq. 30 is linear, the effects of multiple channels superimpose linearly, so the steady-state EBA easily extends to M channels:

$$Ca = \frac{1}{2\pi D_c} \sum_{j=1}^M \frac{\sigma_j \exp(-r_j/\lambda)}{r_j} + Ca_{bk}. \tag{32}$$

In the absence of mobile buffer the rapid buffer and excess buffer formulas are identical. In the presence of buffer the two formulas differ significantly, and the validity of each approximation is determined by the buffer properties. Fig. 3 shows the free Ca^{2+} concentration as a function of the distance from an open Ca^{2+} channel, in the presence (*dashed curves*) and absence (*solid curve*) of a mobile buffer. In one case a 100 μM concentration of buffer is simulated using the RBA (●). In another case a 1 mM buffer concentration is simulated with the EBA (○). As expected, the free Ca^{2+} concentration is lower when the buffer concentration is higher. Throughout this report we use the RBA to simulate the presence of a saturating mobile buffer and the EBA for an unsaturable buffer.

MULTICHANNEL RELEASE MODEL

In this section we extend the transmitter release model to accommodate the effects of more than one Ca^{2+} channel per release site, employing the preceding multichannel steady-state Ca^{2+} formulas. With two channels per site (Fig. 4) the previous kinetic box diagram describing the Ca^{2+} channel/release site complex is replaced by a cube diagram: one dimension for Ca^{2+} binding/unbinding; one dimension for the opening/closing of the first channel; one dimension for the opening/closing of the second channel. Assuming that the kinetic rates are identical for the two channels, the equations describing release are natural extensions of Eqs. 1–5:

$$\frac{dS_0^{pq}}{dt} = k_1^- S_1^{pq} - 4\kappa_1^{pq} S_0^{pq} + F_0^{pq} \tag{33}$$

$$\frac{dS_1^{pq}}{dt} = 4\kappa_1^{pq} S_0^{pq} + 2k_2^- S_2^{pq} - (k_1^- + 3\kappa_2^{pq}) S_1^{pq} + F_1^{pq} \tag{34}$$

$$\frac{dS_2^{pq}}{dt} = 3\kappa_2^{pq} S_1^{pq} + 3k_3^- S_3^{pq} - (2k_2^- + 2\kappa_3^{pq}) S_2^{pq} + F_2^{pq} \tag{35}$$

TABLE 1 Parameter values for buffers and Ca^{2+} diffusion

Symbol	Definition	Value	Reference
D_c	Free Ca^{2+} diffusion coefficient	220 $\mu m^2\ s^{-1}$	Allbritton et al., 1992
D_m	Mobile buffer diffusion coefficient	75 $\mu m^2\ s^{-1}$	Pethig et al., 1989
Ca_{bk}	Bulk Ca^{2+} concentration	0.1 μM	
B_m^T	Mobile buffer concentration	100 μM or 1 mM (if present)	
K_m	Dissociation constant: mobile	0.4 μM	Pethig et al., 1989
k_m^+	Mobile buffer binding rate	600 $\mu M^{-1}\ s^{-1}$	Pethig et al., 1989

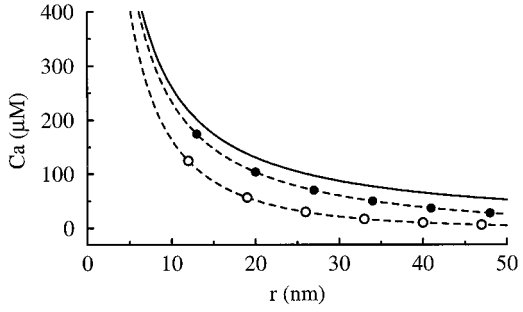

FIGURE 3 Free Ca^{2+} concentration at a release site as a function of the distance from an open Ca^{2+} channel, with membrane potential $V = -65$ mV. The Ca^{2+} profile is computed in the absence of buffer (*solid curve*); in the presence of 100 μM of a mobile buffer using the RBA (*dashed curve with* ●; Eq. 23); and in the presence of 1 mM of a mobile buffer using the EBA (*dashed curve* with ○; Eq. 31). Buffer properties are described in Table 1, and the bulk Ca^{2+} concentration is fixed at 0.1 μM, as in all subsequent simulations.

$$\frac{dS_3^{pq}}{dt} = 2\kappa_3^{pq}S_2^{pq} + 4k_4^-S_4^{pq} - (3k_3^- + \kappa_4^{pq})S_3^{pq} + F_3^{pq} \tag{36}$$

$$\frac{dS_4^{pq}}{dt} = \kappa_4^{pq}S_3^{pq} - 4k_4^-S_4^{pq} + F_4^{pq}, \tag{37}$$

where S_j^{pq} is the probability that a release site has j gates bound and the associated channels are in states p and q, respectively. The forward binding rate $\kappa_j^{pq} = k_j^+ Ca$, where Ca may be computed from either of the multichannel domain Ca^{2+} formulas (Eqs. 28 or 32), with channel distances r_1 and r_2. The channel transition terms F_j^{pq} are derived from the following channel configuration diagram:

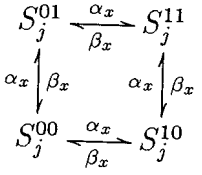

They are:

$$\begin{aligned} F_j^{pq} = {} & h_1(\alpha_x S_j^{00} + \beta_x S_j^{11}) + h_2\alpha_x(S_j^{10} + S_j^{01}) \\ & + (1 - h_1 - h_2)\beta_x(S_j^{10} + S_j^{01}) \\ & - [h_1(\alpha_x + \beta_x) + 2h_2\beta_x + 2(1 - h_1 - h_2)\alpha_x]S_j^{pq}, \end{aligned} \tag{38}$$

where $h_1 = p(1 - q) + q(1 - p)$ and $h_2 = pq$. Release probability is:

$$R = S_4^{00} + S_4^{10} + S_4^{01} + S_4^{11}. \tag{39}$$

As before, the number of differential equations can be reduced using conservation conditions, one for each of the four channel configurations:

$$S_0^{00} + S_1^{00} + S_2^{00} + S_3^{00} + S_4^{00} = (1 - x)^2 \tag{40}$$

$$S_0^{01} + S_1^{01} + S_2^{01} + S_3^{01} + S_4^{01} = x(1 - x) \tag{41}$$

$$S_0^{10} + S_1^{10} + S_2^{10} + S_3^{10} + S_4^{10} = x(1 - x) \tag{42}$$

$$S_0^{11} + S_1^{11} + S_2^{11} + S_3^{11} + S_4^{11} = x^2. \tag{43}$$

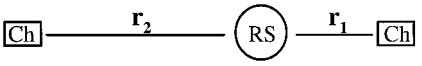

FIGURE 4 In the two-channel model, each release site is associated with two Ca^{2+} channels, located at distances r_1 and r_2 from the site.

The equations for mean release can be extended to M channels per release site. In the most general formulation, with unequal spacing between the release site and the different channels, the number of equations required is $5 \cdot 2^M$ since there are 2^M distinct channel configurations for each of the five gate configurations. The 2^M algebraic conservation laws reduce the number of differential equations to $4 \cdot 2^M$. A much greater reduction in the number of equations is achieved if the channels are constrained to lie at equal distances from the release site (Fig. 5). In this case there are $M + 1$ channel configurations leading to distinct Ca^{2+} levels at the release site, so $5(M + 1)$ equations are required to describe release. Application of the $M + 1$ conservation laws reduces the number of differential equations further to $4(M + 1)$. For example, if there are 10 channels per release site, then the equidistant channels constraint reduces the number of equations from 4096 to 44. Redefining S_j^m as the probability that a release site has j gates bound and m channels open, the equations for release with M equidistant channels are

$$\frac{dS_0^m}{dt} = k_1^-S_1^m - 4\kappa_1^mS_0^m + F_0^m \tag{44}$$

$$\frac{dS_1^m}{dt} = 4\kappa_1^mS_0^m + 2k_2^-S_2^m - (k_1^- + 3\kappa_2^m)S_1^m + F_1^m \tag{45}$$

$$\frac{dS_2^m}{dt} = 3\kappa_2^mS_1^m + 3k_3^-S_3^m - (2k_2^- + 2\kappa_3^m)S_2^m + F_2^m \tag{46}$$

$$\frac{dS_3^m}{dt} = 2\kappa_3^mS_2^m + 4k_4^-S_4^m - (3k_3^- + \kappa_4^m)S_3^m + F_3^m \tag{47}$$

$$\frac{dS_4^m}{dt} = \kappa_4^mS_3^m - 4k_4^-S_4^m + F_4^m, \quad (m = 0, \ldots, M) \tag{48}$$

where $\kappa_j^m = k_j^+ Ca$ and Ca is the Ca^{2+} concentration at the release site with m open channels each at a distance r. The terms F_j^m, derived from the channel configuration scheme

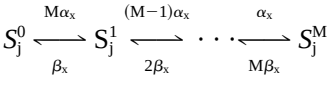

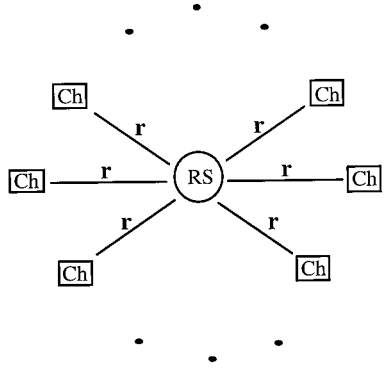

FIGURE 5 In the equidistant-channel model, each release site is associated with M Ca^{2+} channels located at a distance r from the site.

are given by

$$F_j^0 = \beta_x S_j^1 - M\alpha_x S_j^0 \tag{49}$$

$$F_j^m = (M - m + 1)\alpha_x S_j^{m-1} + (m + 1)\beta_x S_j^{m+1} - [(M - m)\alpha_x + m\beta_x]S_j^m, \quad (m = 1, \ldots, M - 1) \tag{50}$$

$$F_j^M = \alpha_x S_j^{M-1} - M\beta_x S_j^M. \tag{51}$$

The release probability is now

$$R = \sum_{m=0}^{M} S_4^m. \tag{52}$$

The equations developed in this section describe the mean release of a system of independent release sites each influenced by Ca^{2+} from two or more Ca^{2+} channels. As an alternate approach, a Monte Carlo simulation could be used to compute the sample mean of release from an ensemble of release sites, as was done in Bertram et al. (1996) for a single-channel release model. This may be preferable in situations where release sites are associated with more than a few non-equally spaced channels.

EFFECTS OF LOCAL CHANNEL GEOMETRY ON FACILITATION

Facilitation is a ubiquitous form of short-term synaptic plasticity which, in our model, is the result of the persistence from one impulse to the next of Ca^{2+} bound to release sites (Fig. 2). In this section we use the multichannel release model to investigate how facilitation and the release time course are affected by the location of the Ca^{2+} channels.

In Fig. 6 each release site is influenced by five Ca^{2+} channels, all located at a distance of 10 nm (*solid curve*) or 50 nm (*dashed curve*). We see from the figure that the shape of the release time course is nearly the same for both channel locations, but facilitation is greater when the channels are located farther from the release site. Similar results hold when 100 μM or 1 mM of a mobile buffer is present and the RBA and EBA are used, respectively, to compute *Ca* (not shown). (These results hold when facilitation is because of slow unbinding of Ca^{2+}; we have not examined what occurs with other mechanisms.) Thus, facilitation is greater under conditions where the Ca^{2+} concentration sensed by the release site is smaller. This relationship, as well as the invariance of the release time course, is similar to what is observed when the external Ca^{2+} concentration is altered. That is, in numerical simulations (Bertram et al., 1996; Bertram and Sherman, 1998; Bennett et al., 1997) and in laboratory experiments it has been shown that the shape of the release time course is unaltered by changes in the external Ca^{2+} concentration (Borst and Sakmann, 1996; Datyner and Gage, 1980) and that facilitation is greater at lower external Ca^{2+} concentrations (Rahamimoff, 1968; Charlton and Bittner, 1978; Stanley, 1986).

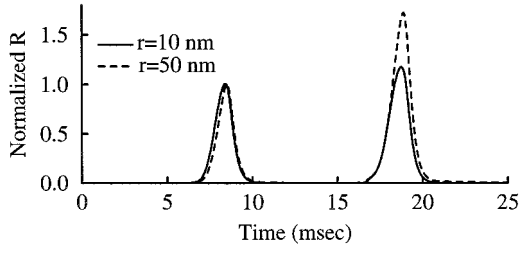

FIGURE 6 Release evoked by two closely spaced action potentials. The peak release during the first response has been normalized to 1. The multichannel release model was used, with five channels per site located at a distance of 10 nm (*solid curve*), or 50 nm (*dashed curve*). The shape of the time course of release is nearly the same with both channel locations, but the facilitation is greater when the channels are more distant. No mobile buffer is present.

Ca^{2+} CURRENT COOPERATIVITY

Experimental studies of transmitter release are limited by the quantities that can be measured or controlled. One measurable quantity is the postsynaptic current (an indicator of the amount of transmitter released). One controllable quantity is the external or bath Ca^{2+} concentration (Ca_{ex}). The relationship between these two quantities has been established in many synapses, where it has been found that $R \propto Ca_{ex}^n$ where n ranges from 1 to 4 (Augustine et al., 1985; Augustine and Charlton, 1986; Borst and Sakmann, 1996; Dodge and Rahamimoff, 1967; Mintz et al., 1995; Reid et al., 1998; Stanley, 1986), suggesting that there are at least four Ca^{2+} binding sites per release site. The implications of different linear and nonlinear dependencies were investigated in earlier theoretical studies (Parnas and Segel, 1981; Parnas et al., 1982).

Complementary to the experimental findings on Ca_{ex} cooperativity are several recent studies that focus on the relationship between transmitter release and the presynaptic Ca^{2+} current (I_{Ca}), often employing Ca^{2+} channel blockers to reduce the Ca^{2+} current. Several of these agents block only specific channel types: ω-conotoxin GVIA, ω-agatoxin IVA, and dihydropyridines block N-type, P-type, and L-type channels, respectively. Others, such as ω-conotoxins MVIIA and MVIIC, ω-agatoxins IA and IIIA, ω-grammotoxin, Ni^{2+}, and Cd^{2+}, appear to block all Ca^{2+} channel types (see Dunlap et al., 1995 for review). In the first case there is selective block of channels, while in the second case the block is random. In either case, results from these manipulations have been used to compute the power relation between transmitter release and I_{Ca}, which we refer to as the Ca^{2+} *current cooperativity of release*: $R \propto I_{Ca}^n$ (Mintz et al., 1995; Wu and Saggau, 1995). In this section we develop formulas that relate the ratio of release before and after channel blockage (the *release ratio*) to the Ca^{2+} current cooperativity, n. These formulas apply to the blockage of any fraction of the population of channels, and to either selective or random blockage. They are generic in the sense that they are based only on the local nature of the Ca^{2+} sources, and not on the Ca^{2+} binding/unbinding kinetics of the release sites.

We begin with the assumption that the release probability is proportional to a power of the presynaptic Ca^{2+} current:

$$R = kI_{Ca}^{n}, \tag{53}$$

where k is a proportionality constant and n is the Ca^{2+} current cooperativity. (I_{Ca} could be replaced with the total Ca^{2+} influx over the course of an action potential, the time integral of I_{Ca} (Mintz et al., 1995). This does not change the results of the analysis in this section.) If a fraction ρ of the Ca^{2+} channels is blocked, then the current is reduced to $(1 - \rho)\, I_{Ca}$, and the release R_ρ is:

$$R_\rho = k(1 - \rho)^n I_{Ca}^{n}. \tag{54}$$

The release ratio, f, is then defined as:

$$f = \frac{R_\rho}{R} = (1 - \rho)^n. \tag{55}$$

Taking the natural logarithm, we obtain a formula relating Ca^{2+} current cooperativity to the release ratio:

$$n = \frac{\ln f}{\ln(1 - \rho)}. \tag{56}$$

The release ratio may be determined experimentally, or it may be computed with a mathematical model. In either case, its value depends on the distribution of blocked channels. At one extreme, the same subset of channels may be blocked at each release site (e.g., only those closest to the release site). At the other extreme, channel blockage may be described by a binomial distribution. In general, if there are two channels per release site, then:

$$f = \mathrm{P}\,[\text{neither blocked}] + \mathrm{P}\,[\text{only ch. 1 blocked}]\, f_{(1)} + \mathrm{P}\,[\text{only ch. 2 blocked}]\, f_{(2)} \tag{57}$$

where P[ ] denotes probability and $f_{(j)}$ is the release ratio following blockage of channel j. Notice that with neither channel blocked the release ratio is equal to one. If both channels are blocked, then release will be gated only by the background bulk Ca^{2+}, and will be negligible. The selectivity of channel blockage is reflected in the probabilities. If the block is random with probability ρ, then

$$\begin{aligned} f &= (1 - \rho)^2 + \rho(1 - \rho)f_{(1)} + \rho(1 - \rho)f_{(2)} \\ &= (1 - \rho)^2 + \rho(1 - \rho)[f_{(1)} + f_{(2)}]. \end{aligned} \tag{58}$$

If the channels are identical and equidistant from the release site, then with random block

$$f = (1 - \rho)^2 f_0 + 2\rho(1 - \rho)f_1 \tag{59}$$

where f_1 is the release ratio with one channel blocked, and $f_0 = 1$. This generalizes to M equidistant channels:

$$f = \sum_{m=0}^{M-1} \binom{M}{m} \rho^m (1 - \rho)^{M-m} f_m \tag{60}$$

where f_m is the release ratio with m channels blocked. If the channels are not equidistant, then a similar formula applies, with f_m replaced by the average of the release ratios for all configurations with m channels blocked. With one channel per release site $f = (1 - \rho)$ and $n = 1$, assuming that the distance between channel and release site is the same at each release site complex. In this case the response is linear, blockage of 50% of the Ca^{2+} current results in a 50% reduction in release.

One prediction that can be made from these cooperativity formulas is that the Ca^{2+} current cooperativity computed through channel blockage is not constant, but depends on the fraction of channels blocked. This can be demonstrated with an example where each release site is associated with two Ca^{2+} channels and the channel blockage is random. By using Eqs. 56 and 58 and taking limits, we see that $n \to 1$ as $\rho \to 1$, and $n \to 2 - (f_{(1)} + f_{(2)})$ as $\rho \to 0$. If the channels are located at distances $r_1 = 10$ nm and $r_2 = 30$ nm from the release sites, then $f_{(1)} = 0.07$ and $f_{(2)} = 0.63$ (see next section). Hence, in this case $n \to 1.3$ as $\rho \to 0$. The Ca^{2+} current cooperativity for this channel configuration is plotted as a function of ρ in Fig. 7 (*bold curve*). Also shown in Fig. 7 are Ca^{2+} current cooperativity curves for several different values of $f_{(1)}$ and $f_{(2)}$, corresponding to different channel locations. Maximal cooperativity is obtained when $f_{(1)} = f_{(2)} = 0$, i.e., when blocking either channel blocks release completely. Then $n = 2$ for all ρ. In the special case where the response to channel blockage is linear, $f_{(1)} + f_{(2)} = 1$ and $n = 1$ for each value of ρ. For all intermediate cases the cooperativity decreases monotonically with ρ. If $f_{(1)} + f_{(2)} > 1$, then $n < 1$ and n increases with ρ (not shown). The lowest possible values of n are obtained when $f_{(1)} = f_{(2)} = 1$, i.e., when blocking either channel has no effect on release because the Ca^{2+} from one open channel is already saturating. This lower bound approaches 0 as $\rho \to 0$.

Some of these results can be extended to the case of M channels per release site. For example, $n \to 1$ as $\rho \to 1$ and $n \to M - \Sigma_j f_{(j)}$ as $\rho \to 0$. If the response to random block

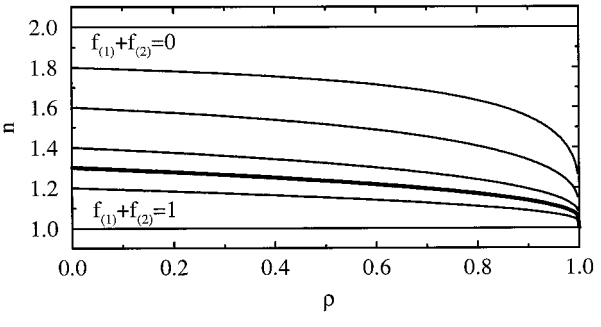

FIGURE 7 The dependence of Ca^{2+} current cooperativity, n, on the fraction of blocked channels, ρ. Each release site is associated with two Ca^{2+} channels. In one example the channels are located at distances $r_1 = 10$ nm and $r_2 = 30$ nm, and $f_{(1)} = 0.07$, $f_{(2)} = 0.63$ (*bold curve*). Other curves correspond to different values of $f_{(1)}$ and $f_{(2)}$, and reflect different channel locations. In two extreme cases there is complete cooperativity $f_{(1)} + f_{(2)} = 0$, or no cooperativity $f_{(1)} + f_{(2)} = 1$.

is linear (i.e., $f_m = (M - m)/M$ in Eq. 60), then $n = 1$ for all ρ. We conjecture that Ca^{2+} current cooperativity remains a decreasing function of the fraction of channels blocked, provided that the response to channel blockage is superlinear ($n > 1$), the most typical case. Finally, maximal Ca^{2+} current cooperativity is obtained when $f_m = 0$ for $m = 1, \ldots, M - 1$. Then $f = (1 - \rho)^M$, and Eq. 56 gives cooperativity $n = M$, the number of channels.

If channel blockage is not random, then the apparent Ca^{2+} current cooperativity can exceed M. For example, if only the closer of two channels (channel 1) per release site is blocked, then $\rho = 1/2$, $f = f_{(1)}$, and $n = \ln(f_{(1)})/\ln(0.5)$. Since $f_{(1)}$ decreases to zero with the distance of the second channel from the release site, the cooperativity n is unbounded. In general, experimental measurements of Ca^{2+} current cooperativity can depend greatly on the distribution of blocked channels. In an extreme case, pharmacological agents may block only those channels too far from release sites to affect vesicle fusion, in which case a reduction in I_{Ca} will have no effect on release. This highlights a conceptual problem that arises when relating changes in presynaptic I_{Ca} to changes in release: changes in the macroscopic quantity I_{Ca} produced by channel blockage do not necessarily reflect similar changes in the Ca^{2+} concentration at the release sites, a microscopic quantity. For this reason, Ca^{2+} current cooperativity measurements will vary greatly according to the distribution of blocked channels. Because this distribution is not easily measured, Ca^{2+} current cooperativity measurements can be difficult to interpret. However, the inverse situation is less ambiguous: assuming that all channels contribute to release and that channel blockage is random, how is Ca^{2+} current cooperativity affected by the number of channels per site and the distance of the channels from the sites? These questions are addressed next.

SENSITIVITY OF RELEASE AND Ca^{2+} CURRENT COOPERATIVITY TO CHANNEL NUMBER AND LOCATION

In this section we use the multichannel release model with the formulas from the previous section to investigate the effects on release of selective and random channel blockage. A range of different channel configurations is examined, both with and without a mobile Ca^{2+} buffer. These simulation data are used to predict how the release ratio and Ca^{2+} current cooperativity vary with channel distance and with the number of channels per site.

We begin with a system employing two channels per release site (Eqs. 33–39), with one channel located at a distance $r_1 = 10$ nm from the site and the other at $r_2 = 30$ nm. Fig. 8 *A* shows release evoked by a single action potential in the absence of mobile buffer with neither channel blocked, with the closer channel blocked (channel 1), and with the farther channel blocked (channel 2). As expected, blockage of the first channel reduces release to a much greater extent than blockage of the second channel,

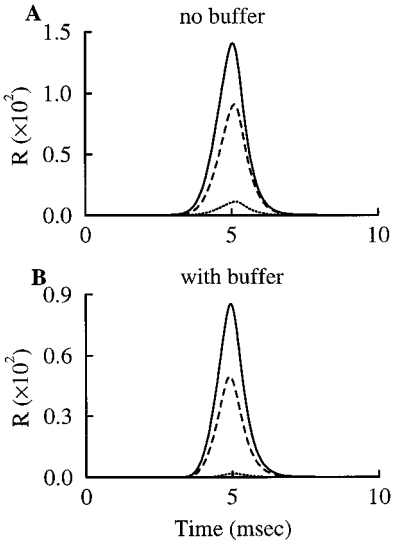

FIGURE 8 Mean release evoked by a single action potential. Each release site has two Ca^{2+} channels, located at distances $r_1 = 10$ nm and $r_2 = 30$ nm. In the control (*solid curve*), neither channel is blocked. Blockage of channel 1 (*dotted curve*) reduces release to a greater extent than blockage of channel 2 (*dashed curve*). (*A*) Without mobile buffer, and (*B*) with 100 μM of a rapid mobile buffer.

with release ratios of $f_{(1)} = 0.07$ and $f_{(2)} = 0.63$, respectively. The release ratio for the random block of 50% of the channels ($\rho = 0.5$) is then determined from Eq. 58 to be $f = 0.43$, intermediate between the selective block of either channel. The Ca^{2+} current cooperativity from random blockage is determined from Eq. 56 to be $n = 1.23$, compared with cooperativities of $n_{(1)} = 3.84$ and $n_{(2)} = 0.67$ for the selective blockage of channels 1 and 2, respectively. This highlights the dependence of Ca^{2+} current cooperativity on the distribution of blocked channels. This example also shows that even though one channel is located significantly farther from the release site than the other, the two work cooperatively in gating release because $n = 1.23$ is greater than the cooperativity $n = 1$ for single-channel release.

The cooperative action of Ca^{2+} channels in gating release is also evident from the observation that $f_{(1)} + f_{(2)} < 1$, or that the sum of the peaks of the dotted and dashed curves in Fig. 8 *A* is less than the peak of the solid curve. This subadditivity is more pronounced in the presence of a saturating mobile buffer (Fig. 8 *B*). In this case, release evoked by channel 2 alone is almost negligible, while the channel's contribution to two-channel release (i.e., the difference between the solid and the dashed curves) is considerable. Indeed, the Ca^{2+} current cooperativity in the presence of buffer is $n = 1.30$, greater than that in its absence. This demonstrates that while distant channels may have little impact on release when acting alone, they can contribute significantly when acting in concert with closer channels.

The release ratio and Ca^{2+} current cooperativity from random channel blockage with various two-channel configurations are summarized in Fig. 9. Here simulations were

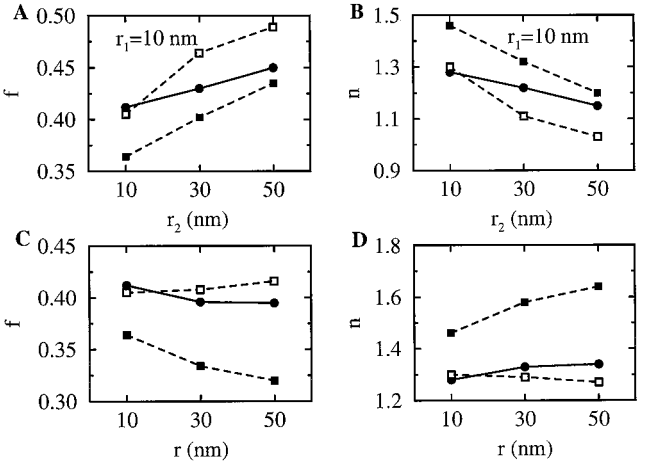

FIGURE 9 Summary of the effects of channel location on the release ratio and Ca^{2+} current cooperativity following channel blockage. In each case *f* and *n* are computed using Eqs. 56 and 60 with random blockage of 50% of the channels. (*A*, *B*) One channel is located at a distance $r_1 = 10$ nm from the release site while the other is placed at various locations. (*C*, *D*) Two equidistant channels are placed at various distances from the release site. Release ratio is lower and Ca^{2+} current cooperativity is greater in the presence of a saturating concentration (100 μM) of mobile buffer (*closed squares*) than in its absence (*solid curves*). However, the presence of an unsaturable concentration (1 mM) of mobile buffer has the opposite effect on the release ratio and Ca^{2+} current cooperativity (*open squares*). The RBA Eqs. 28 and 29 and the EBA Eq. 32 are used for saturating and unsaturable buffers, respectively.

performed in the absence of mobile buffer (*solid curves*); in the presence of a 100 μM concentration of mobile buffer, in which case the buffer saturates and the RBA is used (*dashed curves* with *closed squares*); and in the presence of a 1 mM buffer concentration, in which case the buffer does not saturate and the EBA is used (*open squares*). The top panels show the effects of moving the second channel away from the release site while the first channel remains fixed at a distance $r_1 = 10$ nm. With or without mobile buffer, as channel 2 is moved to greater distances the release ratio increases toward 0.5 and the Ca^{2+} current cooperativity decreases toward 1, the values characteristic of single-channel release. Thus, the influence of the second channel declines, and the role of the closer channel in gating release becomes more prominent. As in Fig. 8, the Ca^{2+} current cooperativity is greatest in the presence of a saturating mobile buffer, regardless of the location of channel 2. However, the cooperativity is lower when an unsaturable buffer is present. Thus, a buffer can have opposite effects on the Ca^{2+} current cooperativity, depending on whether or not it is saturated.

For the lower panels of Fig. 9 the two channels are equidistant, and the effects of moving both away from the release site are examined. In the absence of mobile buffer or in the presence of an unsaturable mobile buffer, the release ratio and the Ca^{2+} current cooperativity are largely insensitive to changes in distance. However, when a saturating mobile buffer is present the release ratio declines and the cooperativity increases toward the upper bound of 2 as channel distance is increased. Thus, when a saturating mobile buffer is present the dependence of release on overlapping Ca^{2+} microdomains is greater when the channels are at a greater distance from the release site.

Fig. 9 reveals a strong dependence of the Ca^{2+} current cooperativity on the saturability of any endogenous or exogenous mobile Ca^{2+} buffers. This is of particular importance since the buffering conditions may vary considerably from synapse to synapse, so differences in cooperativities between synapses may reflect the properties of Ca^{2+} buffers as much as any differences in the local geometry of Ca^{2+} channels.

The dependence of the release ratio and Ca^{2+} current cooperativity on the number of channels per release site is shown in Fig. 10. Each channel is located at a distance $r = 50$ nm from a release site, and simulations were performed in the absence of buffer and in the presence of either a saturating or an unsaturable buffer. In the absence of mobile buffer or in the presence of an unsaturable buffer, the release ratio decreases and cooperativity increases modestly with channel number. When a saturating mobile buffer is present, the decline in release ratio and the rise in cooperativity are accentuated. Thus, as in Fig. 9, the Ca^{2+} current cooperativity depends greatly on whether a buffer is present, and if so, whether or not it is saturated. With six channels per site, Ca^{2+} current cooperativity $n \approx 1.7$ without buffer and $n \approx 2.3$ with a saturating buffer. Both cooperativity

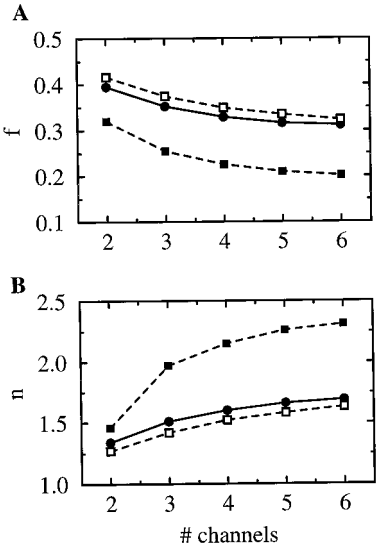

FIGURE 10 The dependence of release ratio and Ca^{2+} current cooperativity on the number of channels per release site. Channels are located at a distance $r = 50$ nm, and values of *f* and *n* are computed using Eqs. 56 and 60 with the random blockage of 50% of the channels. The RBA Eqs. 28 and 29 are used to simulate the presence of a saturating mobile buffer (*closed squares*), while the EBA Eq. 32 is used for an unsaturable mobile buffer (*open squares*). The release ratio is lower and the Ca^{2+} current cooperativity is greater in the presence of a saturating concentration (100 μM) of buffer than in its absence (*solid curves*) or in the presence of an unsaturable concentration (1 mM). The number of channels per site is the theoretical upper bound on the cooperativity obtained through random channel blockage.

values are far below the theoretical upper bound of 6, but well above the Ca^{2+} current cooperativity for single-channel release. A Ca^{2+} current cooperativity of 2.5 was determined experimentally from random channel blockage with Cd^{2+} at the granule cell to Purkinje cell synapse in rat cerebellar slices (Mintz et al., 1995).

Are the results shown in Figs. 9 and 10 consequences of the values of the Ca^{2+} binding/unbinding kinetic rates of the release mechanism? To investigate this question we recomputed the curves in the two figures with three additional sets of kinetic rates. In the first set the Ca^{2+} unbinding rates were made uniformly large ($k_j^- = 2.5\ ms^{-1}$), so that there is no slow unbinding of Ca^{2+} from the release site. In the second set, the original kinetic rates were used, but the $S_4 \rightarrow S_3$ transition was replaced with an $S_4 \rightarrow S_0$ transition, as described earlier. In the third set, the kinetic rates for a model of transmitter release from a ribbon synapse of goldfish retinal bipolar neurons (Heidelberger et al., 1994) were employed. Results obtained with each modified release model exhibited the same trends as those displayed in Figs. 9 and 10 (not shown). Therefore, these trends appear to be robust to modifications of the kinetic structure of the release sites.

DISCUSSION

We have described a mathematical model of transmitter release in which release is gated by the sequential binding to release sites of Ca^{2+} that enters the terminal through nearby Ca^{2+} channels. Unlike our earlier model, where release was influenced by single Ca^{2+} microdomains (Bertram, 1997; Bertram and Sherman, 1998; Bertram et al., 1996), the present model allows for release evoked by the overlapping Ca^{2+} microdomains that form when several channels are open simultaneously. Despite this increased generality, the model remains computationally simple since the Ca^{2+} concentration at the release sites is calculated with equilibrium formulas rather than by solving time-dependent reaction-diffusion equations. These are based on formulas for the equilibrium Ca^{2+} concentration near a single Ca^{2+} channel (Neher, 1986; Smith, 1996), extended to the case of multiple channels. The probabilistic opening of Ca^{2+} channels is handled by deriving equations for the mean release.

This model was used to investigate the effects of channel location on facilitation. We found that facilitation is greater when the Ca^{2+} channels are located farther from the release sites (Fig. 6). In this case, the amplitude of the mean Ca^{2+} signal at the release sites is reduced, while the shape of the signal is not significantly altered. This prediction is consistent with experimental findings that facilitation is increased when the external Ca^{2+} concentration is lowered (Rahamimoff, 1968; Charlton and Bittner, 1978; Stanley, 1986), a procedure that also reduces the amplitude of the mean Ca^{2+} signal without significantly changing its shape.

As another application of the model, we examined the influence of the local channel geometry on the cooperative action of Ca^{2+} channels in gating release. We first derived formulas relating Ca^{2+} current cooperativity to the release ratio following channel blockage. Formulas were also derived relating the release ratio from random channel blockage to a weighted sum of the release ratios from selective channel blockage. The formulas are generic in the sense that they assume only that the Ca^{2+} sources are local to the release sites, and are independent of the kinetics of the Ca^{2+} binding/unbinding kinetics. With these, we showed that the channel number is an upper bound on Ca^{2+} current cooperativity determined through random channel blockage, although no upper bound exists when blockage is selective. These formulas were then used in conjunction with the transmitter release model to investigate how channel distance, channel number, and different concentrations of a mobile buffer affect the release ratio and Ca^{2+} current cooperativity.

Our analysis suggests that great care must be taken in the interpretation of the cooperative relation between release, which is gated by local channel openings, and the presynaptic Ca^{2+} current, which is a macroscopic measure of Ca^{2+} influx. This was demonstrated using a release model with two channels per release site, one situated close to the site and the other farther away (Fig. 8 *A*). Selective block of the closer channel yielded a release ratio of $f_{(1)} = 0.07$, while block of the farther channel yielded $f_{(2)} = 0.63$. Since 50% of the channels were blocked in both cases, these values give cooperativities of $n = 3.84$ and $n = 0.67$, respectively (Eq. 56). This is in contrast to a Ca^{2+} current cooperativity of $n = 1.23$ computed with random blockage of 50% of the channels. Thus, if a Ca^{2+} channel blocking agent is used to measure Ca^{2+} current cooperativity, the measured value depends greatly on the specificity of the agent. This dependence of Ca^{2+} current cooperativity on the blocking agent has been interpreted in terms of the local geometry. For example, in two studies it was found that the Ca^{2+} current cooperativity was higher when the specific P-type Ca^{2+} channel blocking agent ω-agatoxin IVA was used ($n = 4.0$ and $n = 4.1$) than when the specific N-type blocker ω-conotoxin GVIA was used ($n = 2.5$ and $n = 3.5$), suggesting that P-type channels are more closely associated with release sites in these synapses (Mintz et al., 1995; Wu and Saggau, 1994).

Another problem with measuring Ca^{2+} current cooperativity through channel blockage is that the cooperativity depends on the fraction of channels blocked. This was demonstrated for the particular case of two channels per release site in Fig. 7. Here it was shown that the Ca^{2+} current cooperativity is a decreasing function of the fraction of channels blocked. We then deduced that a similar dependence applies for release sites associated with any number of Ca^{2+} channels, at least in the case of equidistant channels. This prediction may be tested in principle by determining Ca^{2+} current cooperativity over a range of concentrations of a Ca^{2+} channel blocking agent.

Although the Ca^{2+} current cooperativity can be used as evidence that release is gated by overlapping Ca^{2+} microdo-

mains in certain synapses, our analysis indicates that Ca^{2+} current cooperativity only provides a lower bound on the average number of channels contributing per release site. For example, in Fig. 10 the Ca^{2+} current cooperativity with six channels per release site is <2 without mobile buffer, and only 2.3 with buffer. In addition, the Ca^{2+} current cooperativity depends greatly on the concentration of mobile buffers in the synapse (Figs. 8–10), a quantity that is not typically known. Finally, it is evident in Fig. 10 that the increase in the Ca^{2+} current cooperativity with the number of channels will saturate. Although the saturation level will depend on many factors, saturation in cooperativity may explain why experimental determinations of Ca^{2+} current cooperativity through random channel blockage rarely exceed 3 or 4 (Wu and Saggau, 1997).

Presynaptic Ca^{2+} current can be reduced either by blocking Ca^{2+} channels or by lowering the external Ca^{2+} concentration (Ca_{ex}). While these procedures have similar effects on the macroscopic current, they have very different effects on single and overlapping Ca^{2+} microdomains. Channel blockage decreases the average number of channels contributing to release per release site, without affecting the Ca^{2+} concentration in single-channel microdomains. In contrast, lowering Ca_{ex} reduces the Ca^{2+} concentration in single-channel microdomains without changing the average number of channels contributing to release. These manipulations have different effects on release, as demonstrated in Fig. 11 using a model with two channels per release site. In one case, the macroscopic Ca^{2+} current is reduced by half by randomly blocking 50% of the Ca^{2+} channels. In the other case, the current is reduced by half by lowering Ca_{ex} from 2 mM to 1 mM. The difference in release results in different cooperativity values; cooperativity obtained through random channel blockage is $n = 1.3$, while that obtained by lowering Ca_{ex} is $n = 2.6$. The Ca_{ex} cooperativity was determined by computing release for several values of Ca_{ex} and plotting $\ln(R)$ vs. $\ln(Ca_{ex})$ (not shown).

It is evident from this example that the cooperative relation between the macroscopic Ca^{2+} current and transmitter release depends greatly on the manner in which the current is varied. If, as in our model, release is gated by the binding of four Ca^{2+} ions, then the cooperativity measured by varying Ca_{ex} has an upper bound of four. This upper bound can be attained even if release is gated by a single Ca^{2+} channel (Bertram et al., 1996). The Ca_{ex} cooperativity value obtained in the present study, $n = 2.6$, is lower than the upper bound because of the binding of basal Ca^{2+} to the Ca^{2+} binding sites. Basal binding may be responsible for the relatively low Ca_{ex} cooperativity values measured in some synapses (Augustine et al., 1985; Mintz et al., 1995; Reid et al., 1998; Stanley, 1986). Thus, measuring cooperativity by varying Ca_{ex} provides information about the Ca^{2+} binding structure of the release sites and the degree of basal saturation. In contrast, if cooperativity is measured by randomly blocking Ca^{2+} channels, then the upper bound is equal to the number of Ca^{2+} channels per release site. For single-channel release, this form of cooperativity has a value of 1 regardless of the number of Ca^{2+} binding sites per release site. Hence, measuring cooperativity by blocking channels provides information about the local channel geometry.

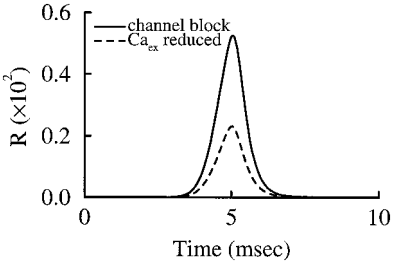

FIGURE 11 The effect on mean release of reducing the presynaptic current by half depends on the manner in which the current is reduced. In one case (*solid curve*), half of the Ca^{2+} channels are randomly blocked. In the other (*dashed curve*), the external Ca^{2+} concentration is reduced from 2 mM to 1 mM. Each release site has two Ca^{2+} channels located at distances $r_1 = 10$ nm and $r_2 = 30$ nm. Release is evoked by a single action potential.

In one experimental study of hippocampal autapses, Ca_{ex} cooperativity was determined in the absence and presence of channel blockers (Reid et al., 1998). That is, Ca_{ex} was varied over a range of values and Ca_{ex} cooperativity determined under different channel blocking conditions. It was found that Ca_{ex} cooperativity was unaffected by the nonselective Ca^{2+} channel blocker Cd^{2+}, but the selective blockers ω-conotoxin and ω-agatoxin significantly reduced the Ca_{ex} cooperativity. Furthermore, Ca_{ex} cooperativity in the presence of ω-conotoxin was approximately the same as Ca_{ex} cooperativity in the presence of ω-agatoxin. The authors suggest that the lower Ca_{ex} cooperativity in the presence of selective blockers is the result of a nonuniform distribution of N- and P/Q-type Ca^{2+} channels. They also point out an apparent discrepancy between their finding that cooperativity in the presence of ω-conotoxin is similar to that in the presence of ω-agatoxin, and the finding by Mintz et al. (1995) that the cooperativity obtained by blocking Ca^{2+} channels with ω-conotoxin is much lower than that obtained by blocking with ω-agatoxin. We suggest that there is no discrepancy, since the cooperativity values obtained by Reid et al. are measurements of Ca_{ex} cooperativity, while the values obtained by Mintz et al. are measurements of Ca^{2+} current cooperativity.

Endogenous mobile Ca^{2+} buffers are ubiquitous in synaptic terminals, and in experimental situations they are often supplemented by exogenous buffers. We have investigated the effects on release and Ca^{2+} current cooperativity of a rapid mobile buffer, with binding kinetics similar to those of the endogenous buffers calbindin-D9k (Klingauf and Neher, 1997) and calmodulin (Falke et al., 1994), and the exogenous buffers fura-2 (Xu et al., 1997) and BAPTA (Pethig et al., 1989). Consistent with experimental data (Adler et al., 1991; Winslow et al., 1994), we found that rapid mobile buffer reduces release (Fig. 8) by lowering the Ca^{2+} con-

centration at the release sites (Fig. 3). In addition, the model predicts that the presence of a saturating mobile buffer increases the Ca^{2+} current cooperativity, that is, the dependence of release on overlapping Ca^{2+} microdomains is greater (Figs. 8–10). Finally, saturating mobile buffer is responsible for giving the Ca^{2+} current cooperativity a positive dependence on equidistant channel distance (Fig. 9) and for increasing the rate of rise of Ca^{2+} current cooperativity with the number of channels per site (Fig. 10). These results suggest that some of the behavior attributed to the transmitter release mechanism may actually be a product of Ca^{2+} buffers.

Other models of secretion from synapses and neuroendocrine cells have employed domain Ca^{2+} as the release trigger (Bennett et al., 1997; Bertram et al., 1996; Klingauf and Neher, 1997). However, ours is the first model to account for overlapping Ca^{2+} domains generated by Ca^{2+} channels whose opening is probabilistic. The sequential Ca^{2+} binding scheme used in the present model is similar in some ways to a model of release for the ribbon synapse of retinal bipolar neurons (Heidelberger et al., 1994). Both models assume four sequential Ca^{2+} binding steps, with graded unbinding rates. However, in the present model the largest unbinding rate is associated with the $S_4 \rightarrow S_3$ transition and the smallest rate is associated with the $S_1 \rightarrow S_0$ transition. The opposite is true in the ribbon synapse model. In addition, all but one of the unbinding rates are significantly smaller in the present model than in the ribbon synapse model, and are the primary mechanism for facilitation.

Like all mathematical models, the present model is based on several assumptions and is subject to several limitations. One assumption is that the Ca^{2+} binding kinetics leading to release are sequential and cooperative, with the graded unbinding rates responsible for facilitation. This cooperative structure is based on electrophysiological data from the squid giant synapse (Bertram et al., 1996; Stanley, 1986) and may require modification for use with other synapses. In any case, the detailed Ca^{2+} binding/unbinding kinetics will ultimately be determined from kinetic data on the vesicle fusion proteins, which is not yet available. A second assumption is that from the releasing state S_4 the release site returns to the partially bound state S_3 rather than the unbound state S_0. During long trains of impulses this could lead to a significant overestimate of facilitation, but we have found that during single impulses or short impulse trains the consequences of this assumption are negligible (not shown). A third assumption is that the store of releasable vesicles does not deplete. Again, this is justified because we look only at release evoked by a single impulse or by short trains, where there should be little depletion. An additional assumption is that Ca^{2+} channels affecting release are situated sufficiently close to the release sites so that the use of equilibrium Ca^{2+} concentration formulas is justified. Modeling studies suggest that this critical distance is $\sim$50 nm, given the Ca^{2+} buffering conditions assumed here (Smith, 1996). However, the present work should be complemented with studies using time-dependent reaction-diffusion equations to compute the Ca^{2+} concentration, both to test the results obtained with the equilibrium formulas and to investigate the effects of channels more distant than 50 nm.

One limitation of the present form of the model is that it cannot be used to simulate the effects of relatively low concentrations of a slow buffer, such as EGTA. This is because of limitations in the Ca^{2+} domain formulas, and could be avoided by solving the time-dependent reaction-diffusion equations. Another limitation is that although the number of equations grows only linearly with the number of equidistant channels, the growth is exponential when no equidistant-channel assumption is made. Thus, with non-equidistant channels it may be preferable to calculate the sample mean of release using a Monte Carlo algorithm (as was done with an earlier model in Bertram et al., 1996).

Details of the structure of active zones in several large synapses are now known (Cooper et al., 1996; Haydon et al., 1994; Heuser et al., 1974; Llinás et al., 1992; Roberts et al., 1990). While we have chosen to investigate generic properties of the release process, it is possible to adapt the transmitter release model described in this report to one or more of these particular synapses. This would require matching the Ca^{2+} channel kinetics and unitary conductance to the Ca^{2+} channel type(s) known to contribute to release in the synapse; specifying the local channel geometry; and finally, adapting the release site Ca^{2+} binding and unbinding rates to fit facilitation data for the particular synapse. Coupling the model to a specific synapse could help bring together morphological and electrophysiological data and thus provide a better understanding of the transmitter release process in this synapse.

APPENDIX

Equations for voltage and Ca^{2+} channel activation

Hodgkin-Huxley equations (Hodgkin and Huxley, 1952) were used to compute the membrane potential:

$$C_m(dV/dt) = -\bar{g}_{Na}m^3h(V - V_{Na}) - \bar{g}_K n^4(V - V_K) - \bar{g}_{leak}(V - V_{leak}) + I_{app} \quad (61)$$

$$dm/dt = \alpha_m(1 - m) - \beta_m m \quad (62)$$

$$dh/dt = \alpha_h(1 - h) - \beta_h h \quad (63)$$

$$dn/dt = \alpha_n(1 - n) - \beta_n n \quad (64)$$

where $\alpha_m = 0.1(V + 40)/[1 - \exp(-(V + 40)/10)]$, $\beta_m = 4\exp[-(V + 65)/18]$, $\alpha_h = 0.07\exp[-(V + 65)/20]$, $\beta_h = 1/[1 + \exp(-(V + 35)/10)]$, $\alpha_n = 0.01(V + 55)/[1 - \exp(-(V + 55)/10)]$, and $\beta_n = 0.125\exp[-(V + 65)/80]$. Values used for the capacitance, current conductances, and reversal potentials are $C_m = 1\ \mu Fcm^{-2}$, $\bar{g}_{Na} = 120\ mScm^{-2}$, $\bar{g}_K = 36\ mScm^{-2}$, $\bar{g}_{leak} = 0.3\ mScm^{-2}$, $V_{Na} = 50$ mV, $V_K = -77$ mV, and $V_{leak} = -54$ mV. Action potentials were induced by an applied current $I_{app} = 30\ \mu Acm^{-2}$ of 1 ms duration.

The domain Ca^{2+} concentration is a function of the single-channel Ca^{2+} current, $i(V)$, which is computed with the Goldman-Hodgkin-Katz formula

(Goldman, 1943):

$$i(V) = \hat{g}_{Ca} P \frac{2FV}{RT}\left[\frac{Ca_{ex}}{1 - \exp(2FV/RT)}\right]. \quad (65)$$

We used $\hat{g}_{Ca} = 12$ pS for the single channel conductance; $P = 6$ mV mM^{-1} for the conversion factor between concentration and membrane potential; $Ca_{ex} = 2$ mM for the external Ca^{2+} concentration; and $RT/F = 26.7$ mV for the thermal voltage. The Ca^{2+} source strength through an open channel is $\sigma = -5.182 \cdot i(V)$ [see the Appendix in Smith et al. (1996)].

The Ca^{2+} channel activation variable x (i.e., the open probability of a channel) is described by

$$dx/dt = \alpha_x(1 - x) - \beta_x x \quad (66)$$

where $\alpha_x = 0.6 \exp(V/10)$ and $\beta_x = 0.2 \exp(-V/26.7)$ are based on voltage clamp data from the squid giant synapse (Llinás et al., 1981a,b).

The authors thank Rodolfo Llinás for suggesting that we look at the effects of channel blockage on release.

REFERENCES

Adler, E. M., G. J. Augustine, S. N. Duffy, and M. P. Charlton. 1991. Alien intracellular calcium chelators attenuate neurotransmitter release at the squid giant synapse. *J. Neurosci.* 11:1496–1507.

Aharon, S., M. Bercovier, and H. Parnas. 1996. Parallel computation enables precise description of Ca^{2+} distribution in nerve terminals. *Bull. Math. Biol.* 58:1075–1097.

Aharon, S., H. Parnas, and I. Parnas. 1994. The magnitude and significance of Ca^{2+} domains for release of neurotransmitter. *Bull. Math. Biol.* 56:1095–1119.

Allbritton, N. L., T. Meyer, and L. Stryer. 1992. Range of messenger action of calcium ion and inositol 1,4,5-trisphosphate. *Science*. 258: 1812–1815.

Augustine, G. J. 1990. Regulation of transmitter release at the squid giant synapse by presynaptic delayed rectifier potassium current. *J. Physiol. (Lond.).* 431:343–364.

Augustine, G. J., E. M. Adler, and M. P. Charlton. 1991. The calcium signal for transmitter secretion from presynaptic nerve terminals. *Ann. N.Y. Acad. Sci.* 635:365–381.

Augustine, G. J., and M. P. Charlton. 1986. Calcium dependence of presynaptic calcium current and post-synaptic response at the squid giant synapse. *J. Physiol. (Lond.).* 381:619–640.

Augustine, G. J., M. P. Charlton, and S. J. Smith. 1985. Calcium entry and transmitter release at voltage-clamped nerve terminals of squid. *J. Physiol. (Lond.).* 367:163–181.

Bennett, M. R., W. G. Gibson, and J. Robinson. 1995. Probabilistic secretion of quanta: spontaneous release at active zones of varicosities, boutons, and endplates. *Biophys. J.* 69:42–56.

Bennett, M. R., W. G. Gibson, and J. Robinson. 1997. Probabilistic secretion of quanta and the synaptosecretosome hypothesis: evoked release at active zones of varicosities, boutons, and endplates. *Biophys. J.* 73:1815–1829.

Bertram, R. 1997. A simple model of transmitter release and facilitation. *Neural Computation.* 9:515–523.

Bertram, R., and A. Sherman. 1998. Population dynamics of synaptic release sites. *SIAM J. Appl. Math*. 58:142–169.

Bertram, R., A. Sherman, and E. F. Stanley. 1996. Single-domain/bound calcium hypothesis of transmitter release and facilitation. *J. Neurophysiol.* 75:1919–1931.

Borst, J. G. G., and B. Sakmann. 1996. Calcium influx and transmitter release in a fast CNS synapse. *Nature.* 383:431–434.

Brose, N., A. G. Petrenko, T. C. Südhof, and R. Jahn. 1992. Synaptotagmin: a calcium sensor on the synaptic vesicle surface. *Science.* 256:1021–1025.

Charlton, M. P., and G. D. Bittner. 1978. Presynaptic potentials and facilitation of transmitter release in the squid giant synapse. *J. Gen. Physiol.* 72:487–511.

Cooper, R. L., J. L. Winslow, C. K. Govind, and H. L. Atwood. 1996. Synaptic structural complexity as a factor enhancing probability of calcium-mediated transmitter release. *J. Neurophysiol.* 75:2451–2466.

Datyner, N. B., and P. W. Gage. 1980. Phasic secretion of acetylcholine at a mammalian neuromuscular junction. *J. Physiol. (Lond.).* 303:299–314.

Davletov, B. A., and T. C. Südhof. 1993. A single C_2 domain from synaptotagmin I is sufficient for high affinity Ca^{2+}/phospholipid binding. *J. Biol. Chem.* 268:26386–26390.

Delaney, K. R., R. S. Zucker, and D. W. Tank. 1989. Calcium in motor nerve terminals associated with posttetanic potentiation. *J. Neurosci.* 9:3558–3567.

Dodge, Jr., F. A., and R. Rahamimoff. 1967. Co-operative action of calcium ions in transmitter release at the neuromuscular junction. *J. Physiol. (Lond.).* 193:419–432.

Dunlap, K., J. I. Luebke, and T. J. Turner. 1995. Exocytotic Ca^{2+} channels in mammalian central neurons. *Trends Neurosci.* 18:89–98.

Falke, J. J., S. K. Drake, A. L. Hazard, and O. B. Peersen. 1994. Molecular tuning of ion binding to Ca^{2+} signaling proteins. *Q. Rev. Biophys. Mol. Biol.* 27:219–290.

Fogelson, A. L., and R. S. Zucker. 1985. Presynaptic calcium diffusion from various arrays of single channels. *Biophys. J.* 48:1003–1017.

Geppert, M., Y. Goda, R. E. Hammer, C. Li, T. W. Rosahl, C. F. Stevens, and T. C. Südhof. 1994. Synaptotagmin I: a major Ca^{2+} sensor for transmitter release at a central synapse. *Cell.* 79:717–727.

Goldman, D. E. 1943. Potential, impedance, and rectifications in membranes. *J. Gen. Physiol.* 27:36–60.

Haydon, P. G., E. Henderson, and E. F. Stanley. 1994. Localization of individual calcium channels at the release face of a presynaptic nerve terminal. *Neuron.* 13:1275–1280.

Heidelberger, R., C. Heinemann, E. Neher, and G. Matthews. 1994. Calcium dependence of the rate of exocytosis in a synaptic terminal. *Nature.* 371:513–515.

Heuser, J. E., T. S. Reese, and D. M. D. Landis. 1974. Functional changes in frog neuromuscular junctions studied with freeze-fracture. *J. Neurocytol.* 3:109–131.

Hodgkin, A. L., and A. F. Huxley. 1952. A quantitative description of membrane current and its application to conduction and excitation in nerve. *J. Physiol. (Lond.).* 117:500–544.

Issa, N., and A. Hudspeth. 1996. The entry and clearance of Ca^{2+} at individual presynaptic active zones of hair cells from the bullfrog's sacculus. *Proc. Natl. Acad. Sci. USA.* 93:9527–9532.

Katz, B., and R. Miledi. 1968. The role of calcium in neuromuscular facilitation. *J. Physiol. (Lond.).* 195:481–492.

Klingauf, J., and E. Neher. 1997. Modeling buffered Ca^{2+} diffusion near the membrane: implications for secretion in neuroendocrine cells. *Biophys. J.* 72:674–690.

Llinás, R., I. Z. Steinberg, and K. Walton. 1981a. Presynaptic calcium currents in squid giant synapse. *Biophys. J.* 33:289–322.

Llinás, R., I. Z. Steinberg, and K. Walton. 1981b. Relationship between presynaptic calcium current and postsynaptic potential in squid giant synapse. *Biophys. J.* 33:323–352.

Llinás, R., M. Sugimori, and R. B. Silver. 1992. Microdomains of high calcium concentration in a presynaptic terminal. *Science.* 256:677–679.

Luebke, J. I., K. Dunlap, and T. J. Turner. 1993. Multiple calcium channel types control glutamatergic synaptic transmission in the hippocampus. *Neuron.* 11:895–902.

Magleby, K. 1987. Short-term changes in synaptic efficacy. *In* Synaptic Function. G. M. Edelman, L. E. Gall, W. Maxwell, and W. M. Cowan, editors. Wiley, New York. 21–56.

Mintz, I. M., B. L. Sabatini, and W. G. Regehr. 1995. Calcium control of transmitter release at a cerebellar synapse. *Neuron.* 15:675–688.

Naraghi, M., and E. Neher. 1997. Linearized buffered Ca^{2+} diffusion in microdomains and its implications for calculation of $[Ca^{2+}]$ at the mouth of a calcium channel. *J. Neurosci.* 17:6961–6973.

Neher, E. 1986. Concentration profiles of intracellular calcium in the presence of a diffusible chelator. *In* Calcium Electrogenesis and Neuro-

nal Functioning. U. Heinemann, M. Klee, E. Neher, and W. Singer, editors. Springer-Verlag, Berlin. 80–96.

Neher, E., and G. Augustine. 1992. Calcium gradients and buffers in bovine chromaffin cells. *J. Physiol. (Lond.).* 450:273–301.

Parnas, H., J. Dudel, and I. Parnas. 1982. Neurotransmitter release and its facilitation in crayfish. I. Saturation kinetics of release, and of entry and removal of calcium. *Pflügers Arch.* 393:1–14.

Parnas, H., and L. A. Segel. 1981. A theoretical study of calcium entry in nerve terminals, with application to neurotransmitter release. *J. Theor. Biol.* 91:125–169.

Pethig, R., M. Kuhn, E. Payne, T. Chen, and L. F. Jaffe. 1989. On the dissociation constants of BAPTA-type Ca^{2+} buffers. *Cell Calcium.* 10:491–498.

Rahamimoff, R. 1968. A dual effect of calcium ions on neuromuscular facilitation. *J. Physiol. (Lond.).* 195:471–480.

Regehr, W. G., and I. M. Mintz. 1994. Participation of multiple calcium channel types in transmission at single climbing fiber to Purkinje cell synapses. *Neuron.* 12:605–613.

Reid, C. A., J. M. Bekkers, and J. D. Clements. 1998. N- and P/Q-type Ca^{2+} channels mediate transmitter release with a similar cooperativity at rat hippocampal autapses. *J. Neurosci.* 18:2849–2855.

Roberts, W. M., R. A. Jacobs, and A. J. Hudspeth. 1990. Colocalization of ion channels involved in frequency selectivity and synaptic transmission at presynaptic active zones of hair cells. *J. Neurosci.* 10:3664–3684.

Sabatini, B. L., and W. G. Regehr. 1996. Timing of neurotransmission at fast synapses in the mammalian brain. *Nature.* 384:170–172.

Simon, S., and R. Llinás. 1985. Compartmentalization of the submembrane calcium activity during calcium influx and its significance in transmitter release. *Biophys. J.* 48:485–498.

Sinha, S. R., L.-G. Wu, and P. Saggau. 1997. Presynaptic calcium dynamics and transmitter release evoked by single action potentials at mammalian central synapses. *Biophys. J.* 72:637–651.

Smith, G. D. 1996. Analytical steady-state solution to the rapid buffering approximation near an open channel. *Biophys. J.* 71:3064–3072.

Smith, A. B., and T. C. Cunnane. 1997. Multiple calcium channels control neurotransmitter release from rat postganglionic sympathetic nerve terminals. *J. Physiol. (Lond.).* 499:341–349.

Smith, G. D., J. Wagner, and J. Keizer. 1996. Validity of the rapid buffering approximation near a point source of calcium ions. *Biophys. J.* 70:2527–2539.

Sneyd, J., P. D. Dale, and A. Duffy. 1998. Traveling waves in buffered systems: applications to calcium waves. *SIAM J. Appl. Math.* 58: 1178–1192.

Stanley, E. F. 1986. Decline in calcium cooperativity as the basis of facilitation at the squid giant synapse. *J. Neurosci.* 6:782–789.

Stanley, E. F. 1993. Single calcium channels and acetylcholine release at a presynaptic nerve terminal. *Neuron.* 11:1007–1011.

Stern, M. 1992. Buffering of calcium in the vicinity of a channel pore. *Cell Calcium.* 13:183–192.

Südhof, T. C., and J. Rizzo. 1996. Synaptotagmins: C_2-domain proteins that regulate membrane traffic. *Neuron.* 17:379–388.

Swandulla, D., M. Hans, K. Zipser, and G. J. Augustine. 1991. Role of residual calcium in synaptic depression and posttetanic potentiation: fast and slow calcium signaling in nerve terminals. *Neuron.* 7:915–926.

Turner, T. J., M. E. Adams, and K. Dunlap. 1993. Multiple Ca^{2+} channel types coexist to regulate synaptosomal neurotransmitter release. *Proc. Natl. Acad. Sci. USA.* 90:9518–9522.

Wagner, J., and J. Keizer. 1994. Effects of rapid buffer on Ca^{2+} diffusion and Ca^{2+} oscillations. *Biophys. J.* 67:447–456.

Wheeler, D. B., A. Randall, and R. W. Tsien. 1994. Roles of N-type and Q-type Ca^{2+} channels in supporting hippocampal synaptic transmission. *Science.* 264:107–111.

Winslow, J. L., S. N. Duffy, and M. P. Charlton. 1994. Homosynaptic facilitation of transmitter release in crayfish is not affected by mobile calcium chelators: implications for the residual ionized calcium hypothesis from electrophysiological and computational analyses. *J. Neurophysiol.* 72:1769–1793.

Wu, L.-G., and P. Saggau. 1994. Pharmacological identification of two types of presynaptic voltage-dependent calcium channels at CA3 to CA1 synapses of the hippocampus. *J. Neurosci.* 14:5613–5622.

Wu, L.-G., and P. Saggau. 1995. Block of multiple presynaptic calcium channel types by ω-conotoxin-MVIIC at hippocampal CA3 to CA1 synapses. *J. Neurophysiol.* 73:1965–1972.

Wu, L.-G., and P. Saggau. 1997. Presynaptic inhibition of elicited neurotransmitter release. *Trends Neurosci.* 20:204–212.

Xu, T., M. Naraghi, H. Kang, and E. Neher. 1997. Kinetic studies of Ca^{2+} binding and Ca^{2+} clearance in the cytosol of adrenal chromaffin cells. *Biophys. J.* 73:532–545.

Yamada, W. M., and R. S. Zucker. 1992. Time course of transmitter release calculated from simulations of a calcium diffusion model. *Biophys. J.* 61:671–682.

Yoshikami, D., Z. Bagaboldo, and B. M. Olivera. 1989. The inhibitory effects of omega-conotoxins on Ca channels and synapses. *Ann. N.Y. Acad. Sci.* 560:230–248.